

Unsupervised Vision and Vision-motion Calibration Strategies for PointGoal Navigation in Indoor Environment

Yijun Cao, Xianshi Zhang, Fuya Luo, and Yongjie Li, *Senior Member, IEEE*

Abstract—PointGoal navigation in indoor environment is a fundamental task for personal robots to navigate to a specified point. Recent studies solved this PointGoal navigation task with near-perfect success rate in photo-realistically simulated environments, under the assumptions with noiseless actuation and most importantly, perfect localization with GPS and compass sensors. However, accurate GPS signal can not be obtained in real indoor environment. To improve the pointgoal navigation accuracy in real indoor, we proposed novel vision and vision-motion calibration strategies to train visual and motion path integration in unsupervised manner. Specifically, visual calibration computes the relative pose of the agent from the re-projection error of two adjacent frames, and then replaces the accurate GPS signal with the path integration. This pseudo position is also used to calibrate self-motion integration which assists agent to update their internal perception of location and helps improve the success rate of navigation. The training and inference process only use RGB, depth, collision as well as self-action information. The experiments show that the proposed system achieves satisfactory results and outperforms the partially supervised learning algorithms on the popular Gibson dataset.

I. INTRODUCTION

Considering how a robot placed in a novel indoor environment can navigate to a target point, e.g., “go 2 meters north, 5 meters west relative to the start”. This task, known as PointGoal navigation, requires the agent to search through the environment unvisited before and approach the target point.

As a basic navigation task in indoor environment, recent methods solve it with near-perfect accuracy (99.6% success) [1] under the assumptions of noiseless egocentric action and accurate localization using GPS and compass sensors. However, these assumptions are difficult to implement in a conventional indoor navigation environment, because the motion process of agents involves physical (e.g., motors and gears), and environmental errors (e.g., collision), which may introduce motion uncertainty to the navigation algorithm. In addition, GPS sensors typically yield an unsatisfactory localization accuracy in indoor environments. Considering these realistic

Yijun Cao, Xianshi Zhang, Fuya Luo and Yongjie Li are with the MOE Key Laboratory for Neuroinformation, the School of Life Science and Technology, University of Electronic Science and Technology of China, Chengdu 610054, China. E-mail: yijuncao@gmail.com, zhangxianshi@uestc.edu, lufuya1993@gmail.com, liyj@uestc.edu.cn. (Corresponding authors: Yongjie Li.)

This work was supported by Guangdong Key R&D Project (2018B030338001) and National Natural Science Foundation of China (61806041, 62076055).

settings, recent researches try to use visual odometry (VO) [2] to replace the GPS sensors or hybrid simultaneous localization and mapping (SLAM) with planning approach [3] for building embedded navigation system. However, these methods still use accurate GPS information as supervision to train their VO or SLAM systems. Thus, in practical indoor applications, it is a promising research direction to train a visual navigation model that completely discards GPS signals.

Navigation only using self-perception is an innate ability of many animals. They are capable of navigating in complex environments, finding food and going back to their nests [4]. Many researches have shown that some neurons in the brain are closely related to the animal’s ability to navigate, for example the place cells [5], head direction cells [6] and grid cells [7]. These cells guide their navigational activities by producing specific responses based on the their specific position and orientation in space. The navigational activities also rely on two fundamental mechanisms: path integration and landmark calibration [8]. Through path integration, animals update their internal neural representations of place using self-motion information. However, the path integration using motion information alone may lead to rapid cumulative errors in both the direction and distance of the goal. Thus, landmark calibration mechanism is further employed to help the animals corrected their cumulative errors caused by the inaccuracy path integration. Inspired by these biological findings, this work proposes novel vision and vision-motion calibration strategies to train visual and motion path integration in unsupervised manner.

Vision calibration implements the function of VO through computing re-projection error from two consecutive frames [9], [10], and replaces the accurate GPS signal with the VO model. In practice, an unsupervised method will encounter two key problems compared with supervised manners. The first one is the scale uncertainty. Monocular RGB images cannot provide the specific scale of motion, e.g., centimeter or meter, so we need depth sensor to provide an absolute scale. Fortunately, depth sensor in indoor environment can provide quite accurate depth information, so we use the noiseless depth to train the model. The second is the accuracy of monocular visual odometry. Compared with supervised methods, the unsupervised algorithm relies only on re-projection error and is therefore difficult to converge to the optimal value. To address this issue, we 1) use richer information to construct re-projection error; 2) propose a novel classified PoseNet (EP-Net) to estimate ego-motion with Linear Motion

(LM) probability volumes which transforms the regression prediction into a probability sum of classification prediction.

Vision-motion calibration strategy helps train the motion path integration (MPI) model by using predicted VO to replace ground truth location as supervised signal. This strategy is based on two key ideas: 1) using a LSTM [11] to compute motion-only path integration, which receives the previous action and collision information, and 2) using accumulative VO as pseudo location label to supervise motion path integration. MPI model can not get an accurate motion path integration due to inputting a noisy action and using inaccurate pseudo label as supervision. Thus, we hope that this component can help visual calibration as auxiliary positioning or teach the intelligent agent to be able to think more about exploration in its next decision, rather than being driven only by the target location. Motivated by the grid cell representation, which proves helpful for PointGoal navigation by making the agent to learn to take shortcuts in some situations [12], we use place and head direction cells to encode the pseudo location label.

To the best of our knowledge, this work is the first method that does not use position signals (GPS+Compass), neither for training nor for inference in learning based PointGoal navigation task. The main contributions are as follows:

- 1) A vision calibration strategy is designed to train a VO model using re-projection error. The VO model is improved by using the proposed CP-Net and richer information to estimate ego-motion.
- 2) The MPI model is proposed and trained based on a vision-motion calibration strategy, which uses the predicted VO as pseudo ground truth label for unsupervised training.
- 3) Experimental results show that the features outputted by the MPI model can significantly improve the navigation performance under the supervision of vision-motion calibration strategy.

On the Habitat simulation platform [13] with Gibson real-world indoor scene dataset [14], our experiments demonstrate that the proposed unsupervised learning algorithm is feasible in PointGoal navigation task and outperforms those partially supervised learning algorithms in quantitative and qualitative comparisons.

II. RELATED WORKS

Learning-based navigation. Conventional navigation methods usually decompose the problem into two separate stages: building a metric or topological map of the environments, and planning a path to the goal [16]. Benefiting from the powerful ability of deep neural networks, many researchers turn to reinforcement learning (RL) [1] or Learning based SLAM [3], [17] to help agents make action decisions. Recently, there has been a renewed interest in the field of embodied navigation tasks in indoor environment, which can be distinguished into PointGoal navigation [1], [2], ImageGoal navigate [18] and ObjectGoal navigation [19], [20]. For PointGoal navigation task, agent is asked to travel to a given coordinate point. To solve this problem, some researchers construct a grid map with SLAM technology, and

use path planning algorithms to find local targets, thereby continuously approximating the global target [3], [17]; others estimate action using RL with visual features and predicted odometry information [2], [21]. ImageGoal and ObjectGoal tasks require intelligent agents to respectively find a specific image and target object, which proposes a greater challenge to explore in unfamiliar environments. Currently, researchers have tried to use dynamically topological maps [18], [20], spatial attention mechanism [22], visual transformer [19], or introduce auxiliary exploration targets [23], [24] to address such two tasks.

Our work is similar to [2], which replaces ground truth GPS+Compass with VO via supervised training. But quite different from that work, we use unsupervised vision calibration strategy to train the VO system and proposed an MPI model with training by vision-motion calibration strategy that further improves navigation success rate under inaccurate VO estimates.

Visual odometry. Visual odometry (VO) is a long-standing problem that estimates the ego-motion incrementally using visual input. Classical geometry-based VO system usually consists of two steps. First, the raw camera measurements are processed to generate a photometric [25] or feature [26] representation. Second, the representation is used to estimate depth and ego-motion using geometry methods (e.g., epipolar geometry and triangulation [26]), and local optimization (e.g., photometric BA [25]). Recently, many researchers have tried to solve the VO problem using CNNs in a supervised or unsupervised manner [27]. The supervised methods minimize the distance between predicted values (depth and ego-motion) and corresponding ground truth by using such strategies as a recurrent neural network (RNN) [28], memory mechanism [29], or feature-metric BA [30]. In contrast, to avoid the need for annotated data, unsupervised VO has been developed using the standard structure-from-motion pipeline. These methods accept continuous image input and infer VO via a CNN [31] or LSTM [32]. To combine the advantages of geometry-based and deep-learning methods, several works [10], [33] tried to learn the various components (e.g., optical flow, depth, and VO) of the entire system to get more accurate performance.

In this work, the unsupervised VO model is based on [27], which used standard structure-from-motion pipeline joint training depth and VO. In addition, we further improve the VO performance with richer visual cues and CP-Net architecture to training more accurate VO.

III. METHOD

A. Overview

The overall architecture of our model is illustrated in Figure 1(a). Considering a set of environments E and point goals G , in each navigation episode, the agent is initialized at random location $\{\rho, \theta\}$ in an environment $e \in E$, where ρ and θ represent respectively the distance and yaw angle related to the goal. At each time step t , the agent predicts an action $a_t \in A$ via a policy network $\pi(vE, pE, aE)$, where vE is visual embedding which receives current depth map and is encoded by a fully connected layer after ResNet18 [15];

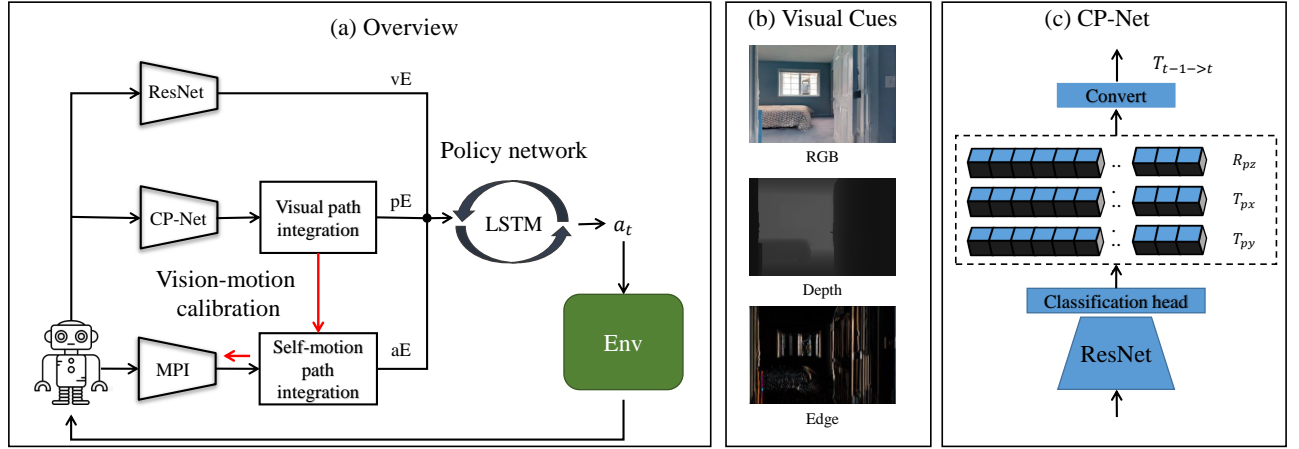


Fig. 1. (a) The policy network is a 2-layer LSTM, which receives observational visual embedding (vE), current position embedding (pE), and previous action embedding (aE). vE is encoded by ResNet18 [15]; pE provides position information which is predicted by the proposed CP-Net with visual path integration; aE provides action and self-motion information which is predicted by the proposed MPI model with self-motion path integration. The red arrows indicate that the MPI model uses the results of the visual model for calibration. (b) Visual cues. We use RGB, depth and vertical edge of RGB image as the visual cues for training our unsupervised VO model. (c) The proposed CP-Net. The CP-Net is composed of a ResNet18 [15] and a classification head activated by SoftMax function, mapping the input two frames to (LM) probability volume $f: I_{t-1}, I_t \rightarrow \{R_{pz}, T_{px}, T_{py}\}$. Then, the probability volume is converted to a rotation and a translation in 2D plane.

pE is position embedding which receives the current position p_t predicted by the proposed VO model and encoded by a fully connected layer; aE is action embedding which receives previous action a_{t-1} , previous collision signal co_{t-1} and is encoded by the proposed motion path integration model. The agent computes a distribution over an action space $A = \{\text{move forward, turn left, turn right, stop}\}$, and the translation and rotation steps are set to $0.25m$ and 10° , respectively. The success of object navigation task requires the agent finally to get close to the point goal (less than a threshold).

B. Unsupervised vision calibration

In this work, visual calibration is implemented as a process of unsupervised VO training. At each time step t , the VO model estimates the rotation $R_{t-1 \rightarrow t}$ and translation $T_{t-1 \rightarrow t}$ between $t-1$ and t in a 2-dimension (2D) plane. Given the previous position ($\hat{P}_{t-1} \in \mathcal{R}^2$), current position can be formulated as:

$$\hat{P}_t = R_{t-1 \rightarrow t} \hat{P}_{t-1} + T_{t-1 \rightarrow t}. \quad (1)$$

Given the position \hat{P} at each time step, we convert it to the distance and direction related to the target goal, and then output pE encoding by a linear layer.

Unsupervised learning pipeline. The core of unsupervised training pipeline is to find the corresponding pixels with regard to depth. Given a pair of adjacent observations I_t and $I_{t'}$, for a coordinate of pixel c_t in I_t , the corresponding pixel $c_{t'}$ in $I_{t'}$ can be found through camera perspective projection for static scenes. Formally, the relationship can be written as

$$c_{t'} = K(R_{t \rightarrow t'} D_t(c_t) K^{-1} c_t + T_{t \rightarrow t'}), \quad (2)$$

where K is the camera intrinsic, and $D_t(c_t)$ denotes the depth at the coordinate c_t . $R_{t \rightarrow t'}$ and $T_{t \rightarrow t'}$ is respectively the rotation and translation of camera pose from time stamp t to t' .

After obtaining the corresponding c_t and $c_{t'}$, the image $I_{t' \rightarrow t}$ can be synthesized using $I_{t'}$ by warping the target coordinate $c_{t'}$ into the source c_t . Then, unsupervised training strategy is realized by minimizing the photometric re-projection error between I_t and the synthetic image $I_{t' \rightarrow t}$:

$$\mathcal{L}_{self} = \frac{1}{|V|} \sum_{c_t \in V} \min_{t'} r(I_t(c_t), I_{t' \rightarrow t}(c_t)), \quad (3)$$

where V is the available pixels for computing the error. The function $r(I_t(c_t), I_{t' \rightarrow t}(c_t))$ is the metric between the source image $I_t(c_t)$ and the synthetic image $I_{t' \rightarrow t}(c_t)$. Similar to [34], the metric is defined as mean absolute error (MAE) with SSIM [35]; $I_{t'}$ contains two adjacent temporal frames around I_t , i.e., $I_{t'} \in \{I_{t-1}, I_{t+1}\}$.

Training with richer visual cues. Conventional unsupervised learning methods [10], [34] use RGB image $I = [R, G, B]_t \in \mathcal{R}^{H \times W \times 3}$ as synthesized target. For estimating more accurate pose, we use richer visual cues as metrics between synthetic and original targets. The first cue is depth. The advantage is that depth information is not easily disturbed by luminance and complex textures. The second cue is structured texture. Considering that the robots can only move on the ground, the edge information in the vertical orientation has the greatest visual discrimination and therefore also facilitates the distinction between the synthetic and the original targets. Inspired by the primary visual cortex of biological visual system which can fast extract multi-scale and multi-orientation edges, we use the bio-inspired contour detection model [36] to detect vertical edges as a kind of auxiliary visual cue. In summary, the synthesized target consists of RGB image, depth map and vertical edges of RGB image:

$$I = [RGB, depth, edge] \in \mathcal{R}^{H \times W \times 7}, \quad (4)$$

$$\text{edge} = RGB(x, y) * \frac{\partial g(x, y, \theta_g, \sigma)}{\partial x},$$

where the symbol $*$ denotes the convolution operation; $\theta_g = \pi/2$ and $\sigma = 1.0$ for extracting vertical edge with fine scale. In addition, our experiment has shown that SSIM is not suitable for measuring differences in depth and edges, because the local averaging of this operation leads to less differentiation in local images. So the total metric function in this work is defined as:

$$r(\Delta I) = \sum_{C \in I} \begin{cases} \alpha MAE(\Delta C) + \beta SSIM(\Delta C) & C = RGB; \\ \gamma MAE(\Delta C) & \text{otherwise,} \end{cases} \quad (5)$$

where $\alpha = 0.15$, $\beta = 0.85$, $\gamma = 1.0$, ΔI and ΔC are abbreviations for $(I_t, I_{t \rightarrow t})$ and $(C_t, C_{t \rightarrow t})$, respectively.

Network. The proposed CP-Net, as shown in Figure 1(c), is composed of a ResNet18 [15] as encoder with two frames as inputs, and several convention layers and full connected layers as classification head. The classification head first maps the features from ResNet18 to three grouped vectors, $f : I_{t-1}, I_t \rightarrow \{R_z, T_x, T_y\}$. Then, these vectors are processed respectively through a *SoftMax* operation along the channel axis to obtain the Linear Motion (LM) probability volume $\{R_{pz}, T_{px}, T_{py}\}$. A sum of the $\{R_{pz}, T_{px}, T_{py}\}$, weighted by the linear motion level value $\{l_r, l_{t_x}, l_{t_y}\}$, represents the rotation around z-axis, and the translation alone x- and y-axis, respectively. The final predicted ego-motion $T_{t-1 \rightarrow t} \in \mathcal{SE}(2)$ is specified by a rotation and a translation at the ground plane,

$$T_{t-1 \rightarrow t} = [R'_{pz}, T'_{px}, T'_{py}] = [l_r R_{pz}^\top, l_{t_x} T_{px}^\top, l_{t_y} T_{py}^\top], \quad (6)$$

where l_r , l_{t_x} and l_{t_y} are arithmetic sequences generated by function *linspace*(*start*, *stop*, *steps*) with the parameters of start value, end value and step size. According to the statistics for the VO dataset (shown in the Supplementary Material), we found that the robot's motion is within a fixed range when it is given a certain motion command. Thus, the parameters of l_r , l_{t_x} and l_{t_y} are set to $(-0.4, 0.4, 81)$, $(-0.25, 0.25, 51)$, $(-0.1, 0.4, 51)$, respectively. The LM probability volume can be understood as a way of pose discretization. Previous works [9], [34] generally regard the pose estimation as a regression model, which uses a CNN to predict the orientations and translations. In contrast, based on the statistics of agent's movements, the proposed CP-Net splits all possible movement amplitudes to small bins and then predicts their probabilities. According to our experiments, this operation can obtain better numerical accuracy than regression model, which may be due that the refined small bins have greater discriminatory power around the optimal value.

C. Vision-motion calibration

Existing work [1], [2] only use previous action as currently moving cues to train the policy. Inspired by mammal's spatial localization mechanisms [7], [8], we argue that motion path integration (MPI) might help to improve the navigation task. This has been preliminarily validated by [12], which use translational and angular velocity as inputs and train a grid cell representations using LSTM with supervision. The representations endow agents with the ability to perform vector-based navigation and improve the convergence speed of policy network.

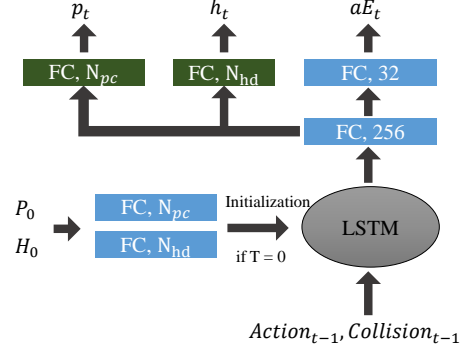


Fig. 2. The proposed motion path integration (MPI) model. The model inputs are previous action and collision, the outputs are p_t , h_t and action embedding aE where p_t and h_t are the predicted place and head-direction cell representations, respectively. The subscript t indicates the t -th moment of recurrent LSTM. P_0 and H_0 are initialized representations of place, and head-direction cell, respectively.

In this work, we proposed the vision-motion calibration that use pseudo trajectory obtained by vision to correct motion integration. Specifically, we use a LSTM to model MPI, as shown in figure 2. The network is required to update its estimate by processing discrete action and collision signals at previous time step $t - 1$. MPI model is not only supervised by pseudo position label (predicted by VO model), but also updated by task driven policy gradient.

Neural Representations. Typical place and direction are represented respectively as Cartesian coordinates and angles. However, such representations are not consistent with place and head-direction cells in mammals [37], [38]. Inspired by [12], we use a neurocompatible encoding method to encode the raw format as a neural vector representation.

Place cell activations $P \in [0, 1]^{N_{pc}}$, encoded from Cartesian coordinates $\mathcal{X} = (x, y)$, are simulated by a 2-D gaussian function with standard deviation σ activated by SoftMax function, written as

$$P^i = \text{softmax}(-(\mathcal{X} - \vec{\mu}_p^i)^2 / 2\sigma^2) \quad (7)$$

where $\vec{\mu}_p \in \mathbb{R}^{N_{pc}}$ are N_{pc} two-dimensional vectors chosen uniformly before training, and $\sigma = 0.5$, the place cell scale, is a positive scalar fixed before training. For ensuring that this representation can cover the whole environment, the places are uniformly distributed throughout the environment. In our experiments, the range of (x, y) in Gibson dataset is $[-25, 25]$, and thus the number N_{pc} is determined by σ : $N_{pc} = ((25 * 2) / 5\sigma)^2$.

For a given angle θ , head-direction cell activations $H \in [0, 1]^{N_{hd}}$, are represented by a Von Mises distribution activated by SoftMax function,

$$H^i = \text{softmax}(e^{k \cos \pi(\theta - \vec{\mu}_h^i) / 180}), \quad (8)$$

where $k = 20$, $N_{hd} = 12$, direction centers $\vec{\mu}_h \in [0, 360)$ are chosen uniformly before training.

Network. As shown in figure 2, the input of the proposed model is discrete action $a_{t-1} \in \mathcal{R}^4$ and collision $co_{t-1} \in \mathcal{R}^2$, which are respectively encoded as a vector using embedding layer. The hidden states of the LSTM, l_0 and m_0 , are initialized

respectively by computing a fully connected layer of the ground truth neural vector representation of place P_0 and head-direction H_0 cells at time 0. Note that the position is initialized as the GPS signal at the first time step, and the direction is initialized as zeros.

The LSTM outputs are sent to a fully connected layers with 256-D outputs. The outputs of the proposed model consists of three branches, one of them computes the action embedding aE as the input of policy network. The other two predict respectively the place and head-direction cell activations, activated by SoftMax function with N_{pc} -D and N_{hd} -D outputs.

Loss. Given the pseudo position P encoded using vector representation, the vision-motion calibration loss is defined as

$$\mathcal{L}_{vc} = \omega_{pc}\mathcal{L}_{pc} + \omega_{hd}\mathcal{L}_{hd}, \quad (9)$$

where \mathcal{L}_{pc} is the cross-entropy loss between pseudo position P_t and MPI output p_t at each time step t ; \mathcal{L}_{hd} is the cross-entropy loss between pseudo direction H_t and MPI output h_t at each time step t . Both ω_{pc} and ω_{hd} are set to 0.05.

D. Navigation policy

The navigation policy (Figure 1) consists of a 2-layer LSTM [11], which receives observational visual feature vE , action embedding aE outputted by proposed MPI model, and position embedding pE predicted by proposed VO model. At each time step t , the policy $\pi(\cdot)$ operates on these features and computes a distribution over the action space A . To learn the policy, we use the DD-PPO algorithm [1] and the same set of hyper-parameters and reward shaping settings.

IV. EXPERIMENTS

A. Experimental setup

We conducted experiments on the Habitat simulator [13] with the Gibson dataset [14]. All models were trained with 72 scenes with the Gibson-4+ dataset, and evaluated on 14 unseen scenes according to the split used in [13]. The agent was equipped with an RGB-D camera mounted at a height of 0.88m. It has a 70° field of view and records egocentric observations with a resolution of 192 × 341 pixels for policy network and 256 × 256 pixels for VO model. The action space A consists of four actions: *move forward* ($\sim 0.25m$), *turn left* and *turn right* ($\sim 10^\circ$), and *stop*. The agent exhibits actuation action noise modeled by LoCoBot robot [39]. During collisions, the "sliding" behavior that allows the agent to slide along the obstacle instead of stopping is disabled.

To train the VO model, we created a dataset of 100,000 steps from 13,036 trajectories randomly sampled from 72 training scenes. Each step consists of an observation with RGB-D sensor. The data collection process includes the following two steps: 1) randomly sampling a starting position and orientation of the agent and a navigable PointGoal in the scene; 2) collecting the shortest path to navigate from the starting point to the point goal. After the VO model is trained, we fix the VO module and fine-tune the policy network with vision-motion calibration loss by using the pre-trained model from [1].

Two evaluation metrics are used: the success rate (SR) and success weighted by path length (SPL) [40]. The navigation is

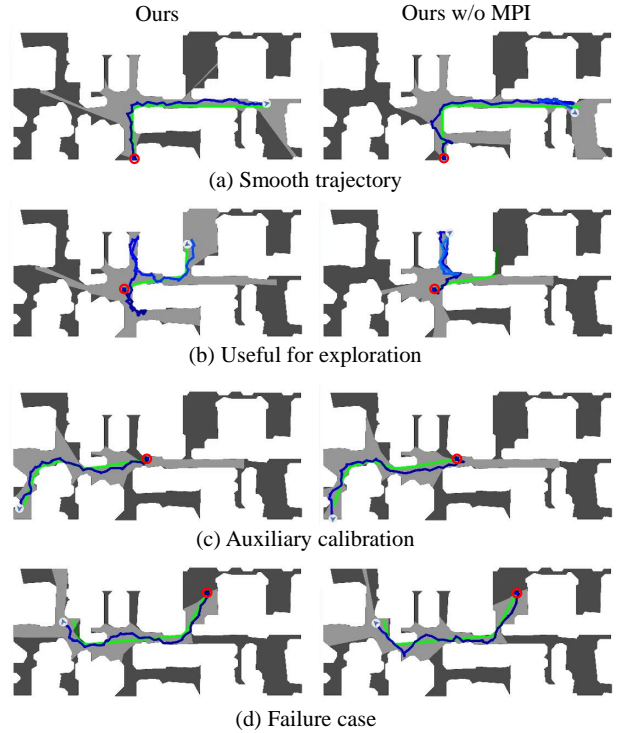


Fig. 3. Visualization of four PointGoal navigation episodes in the *Cantwell* scene. Red circle, green line and blue line indicate starting point, ground truth trajectory and predicted action trajectory, respectively. The position and direction of blue arrow indicate the position and orientation of the robot in its final time step.

successful ($S = 1$) when the agent takes the stop action within 0.36m around the target location. SPL represents the efficiency of a navigation path $SPL = \frac{1}{E} \sum_{i=1}^E S_i \frac{l_i}{\max(l_{a_i}, l_i)}$, where E is the total number of evaluation episodes; $S_i \in \{0, 1\}$ represents whether the agent succeeded ($S_i = 1$) in reaching the target location at the i -th episode or not ($S_i = 0$); l_i and l_{a_i} are the shortest path distances to the target location and the actual path length taken by the agent, respectively. SoftSPL replaces the binary success S_i with a progress indicator $(1 - \frac{d_G}{d_{init}})$ that measures how close the agent gets to the target global coordinate at episode termination, where distance to goal (d_G) captures the geodesic distance between the agent and the goal upon episode termination averaged across all episodes; d_{init} is the starting geodesic distance to the goal.

B. Quantitative results

Compared with state-of-the-art. Table I shows the quantitative results of the proposed and compared methods on the Gibson-4+ validation set [14]. Evaluation and conducted on 994 episodes from 14 validation scenes, each of which provides 71 episodes. DeepVO [41] is a classical supervised RNN-based VO method. Compared with DeepVO, our model shows an improvement of the success rate by 43.8% (from 50 to 71.9) and SPL by 31.3% (from 39 to 51.2). By comparing the results of the proposed model and SLAM-net [3], which is a state-of-the-art SLAM based navigation method, we can see that our algorithm still has advantage for the success rate by 10.6% (from 65 to 71.9) and SPL by 34.7% (from 38 to

TABLE I

EVALUATION OF THE PREVIOUS SUPERVISED METHODS AND OUR MODEL ON THE GIBSON-4+ VALIDATION SPLIT. SUP. AND UNSUP. INDICATE SUPERVISED TRAINING AND UNSUPERVISED TRAINING. SR, SPL, AND SOFTSPL ARE REPORTED IN %.

Method	Train	SR↑	SPL↑	SoftSPL↑
DeepVO [41]	Sup.	50 \pm 1	39 \pm 1	65 \pm 0
SLAM-net [3]	Sup.	66	38	-
supVO-base [2]	Sup.	61 \pm 1	46 \pm 1	62 \pm 1
supVO-full [2]	Sup.	82 \pm 1	63 \pm 1	71 \pm 0
Ours	UnSup.	71.9 \pm 1.8	51.2 \pm 1.3	63.2 \pm 0.6

TABLE II

ABLATION RESULTS ON THE GIBSON-4+ VALIDATION SPLIT. RECINFO INDICATES WHICH VISUAL CUES ARE USED FOR COMPUTING RE-PROJECTION LOSS. E AS ABBREVIATION FOR VERTICAL EDGE. CP-NET AND FT INDICATE, RESPECTIVELY, WHETHER THE MODEL USE CP-NET WITH LM PROBABILITY VOLUME AND FINE-TUNE THE POLICY NETWORK WITH VO. SR, SPL, AND SOFTSPL ARE REPORTED IN %.

Row	Visual	RecInfo	CP-Net	FT	<i>aE</i>	SR↑	SPL↑	SoftSPL↑
0				Ground-Truth		0.95 \pm 0.7	65.9 \pm 0.7	65.2 \pm 0.4
1	RGB	RGB			Emb.	51.0 \pm 1.4	36.4 \pm 1.0	57.8 \pm 0.7
2	RGB-D	RGB			Emb.	54.1 \pm 2.0	37.2 \pm 1.4	57.5 \pm 0.8
3	RGB-D	RGB-D			Emb.	55.0 \pm 1.7	38.5 \pm 1.0	57.7 \pm 0.7
4	RGB-D	RGB-D+E			Emb.	62.1 \pm 1.5	42.8 \pm 1.0	59.9 \pm 0.7
5	RGB-D	RGB-D+E	✓		Emb.	62.7 \pm 1.6	43.1 \pm 1.1	59.6 \pm 0.6
6	RGB-D	RGB-D+E	✓	✓	Emb.	65.7 \pm 1.9	45.3 \pm 1.3	59.6 \pm 0.7
7	RGB	RGB			MPI	58.5 \pm 1.6	41.2 \pm 0.8	61.0 \pm 0.8
8	RGB-D	RGB-D			MPI	61.0 \pm 1.9	41.4 \pm 1.3	59.1 \pm 0.8
9	RGB-D	RGB-D+E			MPI	68.0 \pm 2.2	47.8 \pm 1.7	62.2 \pm 0.5
10	RGB-D	RGB-D+E	✓	✓	MPI only \mathcal{L}_{vc}	67.7 \pm 2.2	48.1 \pm 1.3	62.6 \pm 0.5
11	RGB-D	RGB-D+E	✓	✓	MPI w/o \mathcal{L}_{vc}	67.4 \pm 2.2	45.7 \pm 1.8	59.6 \pm 0.4
12	RGB-D	RGB-D+E	✓	✓	MPI	71.9 \pm 1.8	51.2 \pm 1.3	63.2 \pm 0.6

51.2). In addition, we split the supVO [2] into two methods for comparison, where supVO-base is the base model (only a network with supervised training) and supVO-full is the full model trained with many tricks, such as action-specific design and depth top-down projection. We can see that in terms of success rate, the proposed method outperforms the supVO-base with RGBD as inputs by 17.9% (from 61 to 71.9), but performs inferior to the supVO-full model.

Ablation study. To better understand the performance of the proposed model, we performed an ablation study in Table II. The components to be evaluated consist of 1) the input type (RGB or RGB-D) of the VO model; 2) the visual information for computing re-projection error (RGB, RGB-D or RGB-D with vertical edge (RGB-D+E)); 3) whether or not to use the proposed CP-Net with LM probability volume; 4) approaches for encoding *aE*, including embedding layer, MPI model and training MPI model with different settings; 5) whether or not to fine-tune the policy network with VO.

In this experiment, we first built a near perfect ground truth of 65.9% SPL with 95% success rate (Row 0 in Table II), which was trained with perfect GPS+Compass sensors under noisy actuation. Under the condition without fine-tuning the policy network, we then trained the VO models separately, and used the VO model as a drop-in replacement for ground truth GPS without any expensive re-training. Because such comparison is more fair, i.e., using only one variable of VO model and not involving the policy network. From the ablation study, we can get several conclusions.

1) *Depth observation helps improve the performances of VO.* In Table II, the RGB-D sensor (Row 2) provides higher navigation success rate and SPL (54.1% SR, 37.2% SPL) compared with RGB-only (Row 1, 51.0% SR, 36.4% SPL).

Furthermore, with MPI model (Rows 7-8), the depth observation also helps improve the performances of VO.

2) *Richer information for computing re-projection error is helpful.* From Rows 2-4 in Table II, we can see that depth sensor (Row 3), as the reconstructed visual cues, slightly improves the success rate by 1.7% (from 54.1 to 55.0) and SPL by 3.5% (from 37.2 to 38.5). Furthermore, using texture information (vertical edge cue) for computing loss (Row 4) significantly improves the success rate by 12.9% (from 55.0 to 62.1) and SPL by 11.2% (from 38.5 to 42.8). In the case of using MPI model (Rows 8-9), the conclusion remains the same.

3) *The proposed CP-Net with LM probability volume is better than direct pose estimation.* Compared with Row 5 and Row 6 (SR 62.1% vs. 62.7%, SPL 42.8% vs. 43.1%), both of them have RGB-D sensor as input and RGB-D with edge as reconstruction target, we can find that the VO model with CP-Net is better than the model without it (using conventional direct pose estimation [34]). The results of Row 9 and 12 (SR 68.0% vs. 71.9%, SPL 47.8% vs. 51.2%) show that the CP-Net also outperforms the direct pose estimation method when taking MPI model for embedding *aE*. In addition, the number of parameters of CP-Net (14.2 million) is only 9.2% more than that of previous method [34] (13.0 million). Note that the proposed CP-Net is only suitable for the movements with specific actions, such as the navigation with discrete action space *A*. Because in this case, the magnitude of the motion is limited and thus can be finely discretized. In more general cases (e.g., the drones with 6 DoF motion), the cost of building LM probability volume (more parameters and slower operation) will be large and more difficult to train.

4) *Tuning policy network with VO further improves per-*

formances. The results in Row 6 exhibits that the VO model was fixed for fine-tuning the policy network using DD-PPO algorithm [1]. The whole process did not use the GPS signal. We can see that compared with Row 5, fine-tuning the policy network further improves the success rate by 4.8% (from 62.7 to 65.7) and SPL by 5.1% (from 43.1 to 45.3).

5) *MPI model significantly improves the performances compared with action embedding layer.* Compared with Row 1 and Row 7 (14.7% improvement in SR), Row 3 and Row 8 (10.9% improvement in SR), Row 4 and Row 9 (9.5% improvement in SR), Row 6 and Row 12 (9.4% improvement in SR), we can clearly see that using the MPI model as the encoding of *aE* significantly improves the navigation performances. In addition, we found that the lower the navigation capability (the less accurate the VO) is, the larger performance boost MPI can give.

6) *The vision-motion calibration loss \mathcal{L}_{vc} is useful for training MPI model.* The results of Row 10 and Row 11 show incomplete training of MPI model. We can find that without \mathcal{L}_{vc} (only receives the policy gradient), The navigation performances will be improved (Row 6 vs. Row 11), but is far inferior to the MPI with \mathcal{L}_{vc} (Row 12). Interestingly, detaching the MPI model and training it only with \mathcal{L}_{vc} (Row 10) can still improve the performance compared with embedding layer (Row 6). This finding may be a side-effect of the fact that encoding position and head direction with neural representation helps improve the performances of navigation.

C. Qualitative results

We show four typical examples of episodes for PointGoal navigation in Figure 3. The first three rows show success cases compared with the method without MPI model (Figure 3(a-c)) . Through our analysis of the navigation results for each episode, we found several typical advantages of MPI, including the ability to better smooth the trajectory of the agent (Figure 3(a)), to better facilitate exploration(Figure 3(b)), and to help the intelligent agent calibrate errors in the visual signal (Figure 3(c)).

We also show a failure case in Figure 3(d). This is a typical failure case that the agent incorrectly estimates the endpoint due to the large accumulated error by VO.

D. Conclusions

This paper demonstrates that it is feasible to train a policy network without using GPS signals in indoor environment. The main solution is to use vision and vision-motion calibration strategies. In vision calibration strategy, we use an unsupervised visual odometry algorithm and further improve the performance by 1) better reconstructing the target image with richer visual cues, e.g., depth and edge, and 2) proposing a CP-Net with LM probability volume using pose discretization manner. In vision-motion calibration strategy, we propose the MPI model to predict action-only odometry using neural representations. The results show that the proposed method achieves satisfactory results and outperforms the state-of-the-art partially supervised learning algorithms on the popular Gibson dataset. Furthermore, the MPI model was demonstrated to

help improve the navigation ability of the intelligent agent under inaccurate positional estimation.

The model in this paper was tested only on the Gibson dataset, which may not provide a comprehensive assessment of the performance of the algorithm, especially the domain adaptation capability. Therefore, our future research will focus on testing and refining the algorithm on a wider range of data and realistic environments.

REFERENCES

- [1] E. Wijmans, A. Kadian, A. Morscos, S. Lee, I. Essa, D. Parikh, M. Savva, and D. Batra, “Dd-ppo: Learning near-perfect pointgoal navigators from 2.5 billion frames,” in *International Conference on Learning Representations*, 2019.
- [2] X. Zhao, H. Agrawal, D. Batra, and A. G. Schwing, “The surprising effectiveness of visual odometry techniques for embodied pointgoal navigation,” in *Proceedings of the IEEE/CVF International Conference on Computer Vision*, 2021, pp. 16 127–16 136.
- [3] P. Karkus, S. Cai, and D. Hsu, “Differentiable slam-net: Learning particle slam for visual navigation,” in *Proceedings of the IEEE/CVF Conference on Computer Vision and Pattern Recognition*, 2021, pp. 2815–2825.
- [4] S. Mandal, “How do animals find their way back home? a brief overview of homing behavior with special reference to social hymenoptera,” *Insectes sociaux*, vol. 65, no. 4, pp. 521–536, 2018.
- [5] J. O’Keefe and D. H. Conway, “Hippocampal place units in the freely moving rat: why they fire where they fire,” *Experimental brain research*, vol. 31, no. 4, pp. 573–590, 1978.
- [6] J. S. Taube, R. U. Muller, and J. B. Ranck, “Head-direction cells recorded from the postsubiculum in freely moving rats. i. description and quantitative analysis,” *Journal of Neuroscience*, vol. 10, no. 2, pp. 420–435, 1990.
- [7] T. Hafting, M. Fyhn, S. Molden, M.-B. Moser, and E. I. Moser, “Microstructure of a spatial map in the entorhinal cortex,” *Nature*, vol. 436, no. 7052, pp. 801–806, 2005.
- [8] A. S. Etienne, R. Maurer, and V. Séguinot, “Path integration in mammals and its interaction with visual landmarks,” *The Journal of experimental biology*, vol. 199, no. 1, pp. 201–209, 1996.
- [9] T. Zhou, M. Brown, N. Snavely, and D. G. Lowe, “Unsupervised learning of depth and ego-motion from video,” in *Proceedings of the IEEE conference on computer vision and pattern recognition*, 2017, pp. 1851–1858.
- [10] Y. Cao, X. Zhang, F. Luo, P. Peng, and Y. Li, “Robust visual odometry using position-aware flow and geometric bundle adjustment,” *arXiv preprint arXiv:2111.11141*, 2021.
- [11] S. Hochreiter and J. Schmidhuber, “Long short-term memory,” *Neural computation*, vol. 9, no. 8, pp. 1735–1780, 1997.
- [12] A. Banino, C. Barry, B. Uriu, C. Blundell, T. Lillicrap, P. Mirowski, A. Pritzel, M. J. Chadwick, T. Degris, J. Modayil *et al.*, “Vector-based navigation using grid-like representations in artificial agents,” *Nature*, vol. 557, no. 7705, pp. 429–433, 2018.
- [13] M. Savva, A. Kadian, O. Maksymets, Y. Zhao, E. Wijmans, B. Jain, J. Straub, J. Liu, V. Koltun, J. Malik *et al.*, “Habitat: A platform for embodied ai research,” in *Proceedings of the IEEE/CVF International Conference on Computer Vision*, 2019, pp. 9339–9347.
- [14] F. Xia, A. R. Zamir, Z. He, A. Sax, J. Malik, and S. Savarese, “Gibson env: Real-world perception for embodied agents,” in *Proceedings of the IEEE conference on computer vision and pattern recognition*, 2018, pp. 9068–9079.
- [15] K. He, X. Zhang, S. Ren, and J. Sun, “Deep residual learning for image recognition,” in *Proceedings of the IEEE conference on computer vision and pattern recognition*, 2016, pp. 770–778.
- [16] S. Thrun, “Learning metric-topological maps for indoor mobile robot navigation,” *Artificial Intelligence*, vol. 99, no. 1, pp. 21–71, 1998.
- [17] D. S. Chaplot, D. Gandhi, S. Gupta, A. Gupta, and R. Salakhutdinov, “Learning to explore using active neural slam,” in *International Conference on Learning Representations*, 2019.
- [18] O. Kwon, N. Kim, Y. Choi, H. Yoo, J. Park, and S. Oh, “Visual graph memory with unsupervised representation for visual navigation,” in *Proceedings of the IEEE/CVF International Conference on Computer Vision*, 2021, pp. 15 890–15 899.
- [19] H. Du, X. Yu, and L. Zheng, “Vtnet: Visual transformer network for object goal navigation,” in *International Conference on Learning Representations*, 2020.

- [20] S. Zhang, X. Song, Y. Bai, W. Li, Y. Chu, and S. Jiang, “Hierarchical object-to-zone graph for object navigation,” in *Proceedings of the IEEE/CVF International Conference on Computer Vision*, 2021, pp. 15 130–15 140.
- [21] S. Gupta, J. Davidson, S. Levine, R. Sukthankar, and J. Malik, “Cognitive mapping and planning for visual navigation,” in *Proceedings of the IEEE Conference on Computer Vision and Pattern Recognition*, 2017, pp. 2616–2625.
- [22] B. Mayo, T. Hazan, and A. Tal, “Visual navigation with spatial attention,” in *Proceedings of the IEEE/CVF Conference on Computer Vision and Pattern Recognition*, 2021, pp. 16 898–16 907.
- [23] J. Ye, D. Batra, A. Das, and E. Wijmans, “Auxiliary tasks and exploration enable objectgoal navigation,” in *Proceedings of the IEEE/CVF International Conference on Computer Vision*, 2021, pp. 16 117–16 126.
- [24] O. Maksymets, V. Cartillier, A. Gokaslan, E. Wijmans, W. Galuba, S. Lee, and D. Batra, “Thda: Treasure hunt data augmentation for semantic navigation,” in *Proceedings of the IEEE/CVF International Conference on Computer Vision*, 2021, pp. 15 374–15 383.
- [25] J. Engel, V. Koltun, and D. Cremers, “Direct sparse odometry,” *IEEE Trans. Pattern Anal. Mach. Intell.*, vol. 40, no. 3, pp. 611–625, 2018.
- [26] R. Mur-Artal and J. D. Tardós, “ORB-SLAM2: an open-source SLAM system for monocular, stereo and RGB-D cameras,” *IEEE Trans. Robot.*, vol. 33, no. 5, pp. 1255–1262, 2017.
- [27] C. Godard, O. Mac Aodha, M. Firman, and G. J. Brostow, “Digging into self-supervised monocular depth prediction,” in *ICCV*, 2019.
- [28] S. Wang, R. Clark, H. Wen, and N. Trigoni, “Deepvo: Towards end-to-end visual odometry with deep recurrent convolutional neural networks,” in *ICRA*, 2017.
- [29] F. Xue, X. Wang, S. Li, Q. Wang, J. Wang, and H. Zha, “Beyond tracking: Selecting memory and refining poses for deep visual odometry,” in *CVPR*, 2019.
- [30] C. Tang and P. Tan, “Ba-net: Dense bundle adjustment network,” in *ICLR*, 2019.
- [31] T. Zhou, M. Brown, N. Snavely, and D. G. Lowe, “Unsupervised learning of depth and ego-motion from video,” in *CVPR*, 2017.
- [32] Y. Zou, P. Ji, Q.-H. Tran, J.-B. Huang, and M. Chandraker, “Learning monocular visual odometry via self-supervised long-term modeling,” in *ECCV*, 2020.
- [33] H. Zhan, C. S. Weerasekera, J. Bian, and I. Reid, “Visual odometry revisited: What should be learnt?” in *ICRA*, 2019.
- [34] C. Godard, O. Mac Aodha, M. Firman, and G. J. Brostow, “Digging into self-supervised monocular depth estimation,” in *Proceedings of the IEEE/CVF International Conference on Computer Vision*, 2019, pp. 3828–3838.
- [35] Zhou Wang, A. C. Bovik, H. R. Sheikh, and E. P. Simoncelli, “Image quality assessment: from error visibility to structural similarity,” *IEEE Trans. Image Process.*, vol. 13, no. 4, pp. 600–612, 2004.
- [36] Y.-J. Cao, C. Lin, Y.-J. Pan, and H.-J. Zhao, “Application of the center-surround mechanism to contour detection,” *Multimedia Tools and Applications*, vol. 78, no. 17, pp. 25 121–25 141, 2019.
- [37] J. S. Taube, “Head direction cells and the neurophysiological basis for a sense of direction,” *Progress in neurobiology*, vol. 55, no. 3, pp. 225–256, 1998.
- [38] E. I. Moser, E. Kropff, and M.-B. Moser, “Place cells, grid cells, and the brain’s spatial representation system,” *Annu. Rev. Neurosci.*, vol. 31, pp. 69–89, 2008.
- [39] A. Murali, T. Chen, K. V. Alwala, D. Gandhi, L. Pinto, S. Gupta, and A. Gupta, “Pyrobot: An open-source robotics framework for research and benchmarking,” *arXiv preprint arXiv:1906.08236*, 2019.
- [40] P. Anderson, A. Chang, D. S. Chaplot, A. Dosovitskiy, S. Gupta, V. Koltun, J. Kosecka, J. Malik, R. Mottaghi, M. Savva *et al.*, “On evaluation of embodied navigation agents,” *arXiv preprint arXiv:1807.06757*, 2018.
- [41] S. Wang, R. Clark, H. Wen, and N. Trigoni, “Deepvo: Towards end-to-end visual odometry with deep recurrent convolutional neural networks,” in *2017 IEEE international conference on robotics and automation (ICRA)*. IEEE, 2017, pp. 2043–2050.